Supporting Information Appendix:

Processive phosphorylation of ERK MAP kinase in mammalian cells.

Kazuhiro Aoki, Masashi Yamada, Katsuyuki Kunida, Shuhei Yasuda, and Michiyuki Matsuda

SI Text

Dephosphorylation rates of ERK in the cytoplasm and nucleus. We determined eight dephosphorylation rates of ERK; i.e., pTpY-ERK→pY-ERK, pTpY-ERK→pT-ERK, pY-ERK→np-ERK, and pT-ERK→np-ERK in each of two compartments, i.e., the cytoplasm and nucleus (Fig. S6). Because several phosphatases, including PTP1B, PP2A, and DUSPs, have reported to be involved in ERK dephosphorylation (1), we attempted to measure the rate constant [/sec] of each dephosphorylation pathway for the cytoplasm and nucleus as the mass of phosphatases. To this end, we established HeLa cell lines stably expressing ERKs tagged with a nuclear export sequences (NES) or a nuclear localization signals (NLS). The cells were treated with EGF followed by an MEK inhibitor, PD184352, to measure the dephosphorylation rates (Fig. S6A, left column). Calyculin A, a serine/threonine phosphatase PP1/PP2A inhibitor, or bpV, a tyrosine phosphatase inhibitor, was also used to discriminate the two dephosphorylation reactions (Fig. S6A, center and right columns). Finally, the time constants for each dephosphorylation pathway were determined by curve-fitting the concentration of phospho-isoforms of ERK with a single exponential decay function (Fig. S6B-K). Notably, we observed accumulation of pT-ERK and pY-ERK in the presence of Calyculin A and bpV, respectively (Fig. S6A). This observation indicated that the dephosphorylation of pTpY-ERK was primarily mediated by serine/threonine phosphatases and tyrosine phosphatases, rather than dual-specificity phosphatases, at least in our experimental conditions. Furthermore, the dephosphorylation rate of MEK was also determined and included in our simulation model (Fig. S7). Of note, we neglected the effect of phosphatase inhibitors on Raf and MEK, because they will not affect the mode of ERK phosphorylation.

Involvement of Scaffold proteins in the processive model. Feasible candidates for the determinant of the processive phosphorylation include scaffold proteins, which regulate assembly of two or more components of signaling pathways and consequently change the mode of phosphorylation (2-6). To examine the contribution of scaffold proteins to the processive phosphorylation, we depleted KSR, MP-1, IQGAP1, Paxillin, or β-arrestin1/2 in HeLa cells by siRNA-mediated gene knockdown (7-11). The depletion of each scaffold protein could affect the phosphorylation efficiency of ERK in HeLa cells stimulated with EGF, but not alter the mode of ERK phosphorylation, namely processive phosphorylation, to the detectable level (Fig. S14). For this reason, at this moment, we failed to obtain any evidence that scaffold proteins cause processive phosphorylation in mammalian cells.

SI Materials and Methods

Plasmids. The cDNA of Xenopus MEK1 or Xenopus ERK2 was inserted into pCXN2-mVenus or pCXN2-mCFP vector to generate pCXN2-mVenus-MEK1, pCXN2-mCFP-MEK1, or pCXN2-mCFP-ERK2 (Fig. S2). Monomeric Venus (mVenus) or CFP (mCFP) was fused at the N-terminus of these vectors. The cDNA of FKBP (12) was introduced into these vectors to obtain pCXN2-mVenus-MEK1-FKBP and pCXN2-mVenus-ERK2-FKBP (Fig. S3). Threonine or tyrosine within the activation loop of ERK2 was replaced with alanine and phenylalanine, respectively, to obtain pCXN2-mVenus-ERK2T188A-FKBP and pCXN2-mVenus-ERK2Y190F-FKBP, respectively (Fig. S3). pCAGGS-FLAG-FRB-NES was designed to express FLAG tag, the FKBP-rapamycin-binding (FRB) domain of the mammalian target of rapamycin, and the nuclear export sequence (NES) of HIV rev protein (LQLPPLERLTLD) from the N-terminus. The cDNAs of human Histon H1 (the kind gift of Dr. Ishikawa) and FRB were prepared by PCR and subcloned into pERedNLS vector (pERedNLS-H1-FRB) (13) (Fig. S3). The cDNA of mouse ERK2 or human MEK1 was subcloned into the modified pCX4bsr or pCX4puro vector (14) to generate pCX4bsr-NES-FLAG-ERK2-mVenus, pCX4bsr-FLAG-ERK2-mCFP-NLS, and pCX4puro-NLS-FLAG-MEK1.
pCX4bsr-NES-FLAG-ERK2-mVenus encoded NES, FLAG tag, ERK2, and mVenus from the N-terminus (Fig. S6). pCX4bsr-FLAG-ERK2-mCFP-NLS was designed to express FLAG tag, ERK2, mCFP and the nuclear localization signal (NLS) of SV40 large T antigen (GGPPKKKPKVEDP). pCX4puro-NLS-FLAG-MEK1 encoded NLS, FALG tag and MEK1 from the N-terminus. A fragment of the kinase-deficient mutant of Xenopus ERK2 (ERK2-KR) was inserted into the pGEX4T3 vector to obtain pGEX4T3-ERK2-KR (Figs. 1, 6, S2, and S5). The cDNA of the wild type Xenopus MEK1 (MEK1WT), constitutively active mutant MEK1 (MEK1SDSE), or human PTP1B (the kind gift of Dr. B. Neel) was subcloned into the pET-12HisFLAG vector, which was designed to express double histidine hexamer-tagged FLAG peptide at the N-terminus (Figs, 1, 6, S2, S4, S5, and S12).

Cells, reagents and antibodies. HeLa cells were purchased from the Human Science Research Resources Bank (Sennan-shi, Japan). HeLa cells were maintained in DMEM (Sigma-Aldrich, St. Louis, MO) supplemented with 10% fetal bovine serum (FBS). HEK-293F cells were purchased from Invitrogen (San Diego, CA), and maintained in FreeStyle 293 Expression Medium (Invitrogen). Expression plasmids were transfected into HeLa cells by 293Fectin (Invitrogen) according to the manufacturer's instructions. EGF was purchased from Sigma-Aldrich. Calyculin A, bpV(phen), ZM336372, and

anisomycin were purchased from Calbiochem (La Jolla, CA). PD184352 was obtained from Toronto Research Chemicals (Ontario, Canada). Phos-tag acrylamide was obtained from the Phos-tag Consortium (http://www.phos-tag.com/). Fluorescent beads for calibration of Venus and CFP were purchased from Invitrogen (InSpeck Green (505/515) Microscope Image Intensity Calibration Kit) and from Polyscience (Fluoresbrite Plain YG 0.1 micron Microspheres) (Warrington, PA). Anti-MEK1/2, anti-ERK1/2, anti-p38, anti-phospho-MEK1/2 (Ser217/221), anti-phospho-ERK1/2 (Thr202/Tyr204 and Thr185/Tyr187, respectively), and anti-phsopho-p38 (Thr180/Tyr182) were purchased from Cell Signaling Technology (Beverly, MA). Anti-cRaf monoclonal antibodies came from BD Transduction Laboratories (San Jose, CA). Anti-pY-ERK and anti-pT-ERK monoclonal antibodies were purchased from Sigma. Anti-GFP and anti-GST rabbit sera were prepared in our laboratory (15, 16). LI-COR blocking buffer, IRDye680- and IRDye800-conjugated anti-rabbit and anti-mouse IgG secondary antibodies were obtained from LI-COR Bioscience (Lincoln, NE). Polyethylene glycol 6000 was purchased from Hampton Research (Aliso Viejo, CA).

Establishment of stable cell lines. For generation of HeLa cell lines stably expressing ectopic proteins, we utilized a retroviral system. The murine ecotropic retrovirus receptor (EcoVR) was first introduced into HeLa cells by retroviruses produced from BOSC23 cells, which had been transfected with pCX4hyg-EcoVR, the packaging plasmid pGP, and the envelope plasmid pVSV-G (14). The HeLa cells stably expressing EcoVR were selected by Hygromycin. Then, HeLa-EcoVR cells were infected with retroviruses obtained from pCX4bsr-NES-FLAG-ERK2-mVenus-, pCX4bsr-FLAG-ERK2-mCFP-NLS-, or CX4puro-NLS-FLAG-MEK1-transfected BOSC23 cells (Fig. S6).

Purification of recombinant proteins and in vitro kinase assay. Recombinant proteins fused to GST-tag and His-tag were expressed in E. coli strain BL21-DE3 from pGEX- and pET-derived vectors and purified as described previously (16). GST-tagged human MEK1, GST-tagged human ERK2, and GST-tagged human cRaf deleted with the N-terminus (kinase active mutant) were purchased from Millipore (Bedford, MA). For preparation of GST-pT-ERK2, plasmids of both pGEX-ERK2-KR and pET-12HisFLAG-MEK1SDSE were cotransformed into E-coli strain BL21-DE3. Fully phosphorylated-GST-ERK2 (pTpY-ERK2) was purified and incubated with recombinant 12HisFLAG-PTP1B to dephosphorylate phospho-tyrosine in dephosphorylation buffer (100 mM Tris [pH 7.5], 100 mM NaCl, 1 mM EDTA, 2 mM DTT). The GST-pT-ERK2 was then further purified. For in vitro kinase assay, GST-ERK2 or GST-pT-ERK2 with 12HisFLAG-MEK1SDSE was incubated in in vitro kinase buffer (50 mM Tris [pH 7.5], 10 mM MgCl2, 0.02% BSA 0.2 mM DTT). The reaction was started by adding 5 x ATP solution (5 mM ATP, 50 mM MgCl2, 25 mM Tris [pH 7.2], 0.15 M NaCl) and stopped at the indicated time point by adding SDS sample buffer.

Preparation of cytoplasmic extract. For preparation of cytoplasmic extract, HEK-293F cells were collected by centrifugation. The packed cells were snap-frozen, followed by rapid thawing in water bath. After centrifugation, the supernatant was collected and used as cytoplasmic extract. The extract was diluted 10-fold for in vitro kinase reaction.

Immunostaining. Cells were fixed with 3.7% formaldehyde and permeabilized with 0.2% Triton X-100. After having been soaked for 1 h in phosphate-buffered saline (PBS) containing 3% BSA and 0.02% Triton X-100, the samples were incubated for 1 h at room temperature with 5 μg/ml anti-pTpY-ERK antibodies, washed with PBS, and then incubated for 30 min at room temperature with Alexa 488 anti-mouse IgG,. The samples were washed with PBS containing 0.2% Tween 20, and imaged with an Olympus FV1000 microscope.

Measurement of the dissociation constant by intermolecular FRET assay. First, images of YFP, CFP and FRET were acquired, and then corrected FRET (cFRET) images were created by subtracting the contributions of cross-excitation and bleed-through as follows:

$$[cFRET] = [FRET] - (0.089 \cdot [YFP]) - (0.55 \cdot [CFP]),$$

where 0.089 and 0.55 indicate the degree of cross-excitation and spectral bleed-through under our microscopic conditions, respectively (17). cFRET and the cFRET/YFP ratio indicate the amount of bound protein and the fraction of acceptor protein that contribute to FRET, respectively. Concentrations of fluorescent proteins were evaluated by calibrated fluorescent beads as described previously (18). The fraction of ERK-bound MEK (Bound MEK/Total MEK) in individual cells was calculated as follows:

$$\frac{Bound\_MEK}{Total\_MEK} = \frac{1}{0.16} \cdot \frac{1}{0.57} \cdot \frac{[cFRET]}{[YFP]},$$

where 0.16 is the maximal FRET efficiency between mVenus-MEK1 and mCFP-ERK2, and 0.57 is a quantum yield of Venus (19). The dissociation constant value was calculated by curve fitting the plotted data with the following equation:

$$\frac{Bound\_MEK}{Total\_MEK} = \frac{[Free\_ERK]}{K_d + [Free\_ERK]},$$

where K_d is a dissociation constant.

In vitro binding assay. Various concentration of GST-ERK2KR and 100 nM 12His-FLAG-MEK1WT were incubated with in vitro binding buffer (PBS, 0.1% Tween-20, 1 mM MgCl2, 40 mM imidazole). Bound protein was pulled down by Ni-NTA agarose beads (Qiagen, Valencia, CA), washed with in vitro binding buffer three times, and eluted with 200 mM imidazole-containing PBS. Each eluate was analyzed by SDS-PAGE and western blotting.

Surface plasmon resonance assay. Surface plasmon resonance spectroscopy was performed with a BIAcore-X optical biosensor instrument (Biacore AB, Uppsala, Sweden)

using a NTA sensor chip (NTA bound to a solid support) as described previously (20). Briefly, surface plasmon resonance buffers were as follows: (i) regeneration buffer: 10 mM Hepes, 0.15 M NaCl, 0.35 M EDTA, pH 7.4; (ii) nickel buffer: 500 μM NiSO4 in running buffer; (iii) running buffer: PBS with 1 mM MgCl2, 0.1 % (v/v) Surfactant 20, pH 7.4. Ligand (12His-tagged MEK1WT) and analyte (GST-tagged ERK2KR) were dissolved in running buffer. All reactions were done at 25 °C. The data were analyzed using BIAevaluation 3.0 software (Biacore AB) and kinetic analyses of primary sensorgrams were carried out by global fitting using a modified-heterogeneous binding model to consider non-specific binding of the analyte to Ni-NTA chip sensor.

Nucleocytoplasmic shuttling rates of MEK and ERK. To measure nuclear import and export rates, we used a rapamycin-induced dimerization system of an FK506-binding protein (FKBP12 or FKBP) and FRB domain. For measurement of nuclear import rates, Histon H1-fused FRB (H1-FRB) was employed as a binder for FKBP-fused proteins. Similarly, the nuclear export rate of ERK was determined with an FRB fused to the nuclear export sequence (NES). We measured nuclear import and export rates of phospho-isoforms of ERK as follows: phosphorylation of ERK2T188A or ERK2Y190F was induced by the stimulation of EGF and bpV for 10 min. Then, Rapamycin was added to the cells in order to trap phosphorylated ERK in nucleus or cytoplasm. The fraction of phospho-isoforms of ERK was measured by Phos-tag Western blotting analysis (Fig. S3A). We utilized this fraction value for the exponential curve fitting. Furthermore, the contribution of MEK-dependent active nuclear export of ERK was ignored, because the nuclear import rate of MEK (4.0×10^{-4} [/sec]) was considerably slower than the nuclear import and export rates of ERK under the time scale used in our simulation model (~30 min). From these data, we show that pTpY-ERK seems to be actively imported into the nucleus. Unexpectedly, the nuclear export rate of pT-ERK is larger than those of the other phospho-isoforms. Thus, both the fast import of pTpY-ERK and the fast export of pT-ERK contribute to the increase in pTpY-ERK accumulation in HeLa cells.

Phosphorylation rates of ERK in vitro. Each experiment included a series of diluted GST-ERK concentration as shown in Fig. S5. These eluates were subjected into Phos-tag western blotting. The amounts of phospho-isoforms of ERK were quantified and fitted by global least-square regression algorithm to solutions of following differential equations with Microsoft Excel Solver:

$$d[np-ERK]/dt = -kf_1 \cdot [MEK] \cdot [np-ERK]$$
$$d[pY-ERK]/dt = kf_1 \cdot [MEK] \cdot [np-ERK] - kf_2 \cdot [MEK] \cdot [pY-ERK]$$
$$d[pTpY-ERK]/dt = kf_2 \cdot [MEK] \cdot [pY-ERK]$$

where [MEK], [np-ERK], [pY-ERK], and [pTpYhK] are concentration of MEK, np-ERK, pY-ERK, and pTpY-ERK, respectively. kf1 and kf2 are phosphorylation rate constants [/M/sec], which are enzymatically identical to kcat/Km at substrate concentrations significantly lower than Km. Initial velocity of the phosphorylation was plotted against the substrate concentration (Fig. S5C). The initial velocity was not saturated up to 1.5×10^{-6} M, indicating that the Michaelis constant of the first phosphorylation step is over this range. Therefore, we assumed the linear reaction rates of ERK phosphorylation at least in the range of ERK concentrations.

siRNA for scaffold proteins and quantitative RT-PCR. Scramble siRNA and validated siRNAs for human KSR1 (#1 and #2) were purchased from Invitrogen (San Diego, CA). siRNAs for human MP1, IQGAP1, Paxillin, β-arrestin1, and β-arrestin2 were obtained Santa Cruz Biotechnology (Santa Cruz, CA). HeLa cells were transfected with 20 μM control siRNA or siRNA for a scaffold protein by Lipofectamine RNAiMAX (Invitrogen). Three days after transfection, total RNA was purified by RNeasy Mini Kit (QIAGEN, Hilden, Germany), and reverse-transcribed by High Capacity cDNA Reverse Transcription kit (Applied Biosystems, Foster City, CA) according to the manufacture's protocol. Then, expression levels of scaffold protein and GAPDH were analyzed by SYBR GreenER qPCR SuperMix (Invitrogen) with ABI PRISM7000 Sequence Detection System (Applied Biosystems). Primers used for real time PCR analysis were listed as follows. GAPDH: (Fw) 5'-GAGTCCACTGGCGTCTTCAC-3' and (Rv) 5'-GTTCACACCCATGACGAACA-3', KSR1: (Fw) 5'-TCTCCCACCCTGGACACTT-3' and (Rv) 5'-GAGGAAGAAAGCCCCTGGT-3' MP1: (Fw) 5'-TGTCAGATAGAGATGGAGTACCTGTT-3' and (Rv) 5'-AAACCAGGTCGCAAAGCAT-3', IQGAP1: (Fw) 5'-TGTGCAAAATTCTATGCAGCTT-3' and (Rv) 5'-GGCAGTCACCCCAGAGATAG-3', Paxillin: (Fw) 5'-CAGCAGACACGCATCTCG-3' and (Rv) 5'-GAGCTGCTCCCTGTCTTCC-3', β -arrestin1: (Fw) 5'-ACTATGAAGTCAAAGCCTTCTGC-3' and (Rv) 5'-GGATGACCAGACGCACAGA-3', β -arrestin2: (Fw) 5'-GGAAACTCAAGCACGAGGAC-3' and (Rv) 5'-CTTGTTGGCACCCTCCTTC-3'

Kinetic modeling and numerical simulation. All kinetic reactions were described with mass action kinetics by using CellDesigner (version 4.0 beta) (21) (Fig. 3A, 4A, and S8). Then, the ordinary differential equations and parameters were exported to the MATLAB software (version R2008b or R2010b; The Mathworks Inc., Natick, MA) through Systems Biology Workbench (version 2.7.8) (22). Numerical simulation was performed by MATLAB software with ode23 function. To ensure consistency of simulation results with western blot results, concentration of phospho-isoforms of ERK was represented by summing all ERK species in nucleus and cytoplasm.

3Parameter search and evaluation. Parameter search was performed by using fminseach function in MATLAB (Fig. S11). The target function for parameter search was residual sum of square (RSS) between the experimental data (Fig. 2E and Fig. 4D) and simulation data in distributive model or processive model. The fminsearch function found a parameter set that minimized the RSS value to fit simulation data with experimental data. After finding optimized parameters in each of the distributive and processive models, the RSS value and the

number of parameters for optimization were utilized to calculate Akaike information criterion (AIC) value for ranking which of models was reasonable (23).

SI References

1. Zhou B, Wang ZX, Zhao Y, Brautigan DL, & Zhang ZY (2002) The specificity of extracellular signal-regulated kinase 2 dephosphorylation by protein phosphatases. *J.Biol.Chem.* 277(35):31818-31825.
2. Burack WR & Shaw AS (2000) Signal transduction: hanging on a scaffold. *Curr.Opin.Cell Biol.* 12(2):211-216.
3. Kolch W (2005) Coordinating ERK/MAPK signalling through scaffolds and inhibitors. *Nat.Rev.Mol.Cell Biol.* 6(11):827-837.
4. Levchenko A, Bruck J, & Sternberg PW (2000) Scaffold proteins may biphasically affect the levels of mitogen-activated protein kinase signaling and reduce its threshold properties. *Proc.Natl.Acad.Sci.U.S.A* 97(11):5818-5823.
5. Patwardhan P & Miller WT (2007) Processive phosphorylation: mechanism and biological importance. *Cell Signal.* 19(11):2218-2226.
6. Shaw AS & Filbert EL (2009) Scaffold proteins and immune-cell signalling. *Nat.Rev.Immunol.* 9(1):47-56.
7. Stewart S, *et al.* (1999) Kinase suppressor of Ras forms a multiprotein signaling complex and modulates MEK localization. (Translated from eng) *Mol. Cell. Biol.* 19(8):5523-5534 (in eng).
8. Schaeffer HJ, *et al.* (1998) MP1: a MEK binding partner that enhances enzymatic activation of the MAP kinase cascade. *Science* 281(5383):1668-1671.
9. Roy M, Li Z, & Sacks DB (2005) IQGAP1 is a scaffold for mitogen-activated protein kinase signaling. *Mol.Cell Biol.* 25(18):7940-7952.
10. Ishibe S, Joly D, Zhu X, & Cantley LG (2003) Phosphorylation-dependent paxillin-ERK association mediates hepatocyte growth factor-stimulated epithelial morphogenesis. *Mol.Cell* 12(5):1275-1285.
11. DeFea KA, *et al.* (2000) beta-arrestin-dependent endocytosis of proteinase-activated receptor 2 is required for intracellular targeting of activated ERK1/2. *J Cell Biol.* 148(6):1267-1281.
12. Aoki K, Nakamura T, Inoue T, Meyer T, & Matsuda M (2007) An essential role for the SHIP2-dependent negative feedback loop in neuritogenesis of nerve growth factor-stimulated PC12 cells. *J.Cell Biol.* 177(5):817-827.
13. Aoki K, Nakamura T, Fujikawa K, & Matsuda M (2005) Local phosphatidylinositol 3,4,5-trisphosphate accumulation recruits Vav2 and Vav3 to activate Rac1/Cdc42 and initiate neurite outgrowth in nerve growth factor-stimulated PC12 cells. *Mol.Biol.Cell* 16(5):2207-2217.
14. Akagi T, Sasai K, & Hanafusa H (2003) Refractory nature of normal human diploid fibroblasts with respect to oncogene-mediated transformation. *Proc.Natl.Acad.Sci.U.S.A* 100(23):13567-13572.
15. Ohba Y, Kurokawa K, & Matsuda M (2003) Mechanism of the spatio-temporal regulation of Ras and Rap1. *EMBO J.* 22(4):859-869.
16. Ohba Y, *et al.* (2000) Regulatory proteins of R-Ras, TC21/R-Ras2, and M-Ras/R-Ras3. *J.Biol.Chem.* 275(26):20020-20026.
17. Fujioka A, *et al.* (2006) Dynamics of the Ras/ERK MAPK cascade as monitored by fluorescent probes. *J.Biol.Chem.* 281(13):8917-8926.
18. Sugiyama Y, Kawabata I, Sobue K, & Okabe S (2005) Determination of absolute protein numbers in single synapses by a GFP-based calibration technique. *Nat.Methods* 2(9):677-684.
19. Nagai T, *et al.* (2002) A variant of yellow fluorescent protein with fast and efficient maturation for cell-biological applications. *Nat.Biotechnol.* 20(1):87-90.
20. Baekgaard L, Luoni L, De Michelis MI, & Palmgren MG (2006) The plant plasma membrane Ca2+ pump ACA8 contains overlapping as well as physically separated autoinhibitory and calmodulin-binding domains. *J.Biol.Chem.* 281(2):1058-1065.
21. Kitano H, Funahashi A, Matsuoka Y, & Oda K (2005) Using process diagrams for the graphical representation of biological networks. *Nat.Biotechnol.* 23(8):961-966.
22. Sauro HM, *et al.* (2003) Next generation simulation tools: the Systems Biology Workbench and BioSPICE integration. *OMICS.* 7(4):355-372.
23. Akaike H (1974) A new look at the statistical model identification. . *IEEE Trans. Automatic Control* 19(6):716-723.

Fig. S1

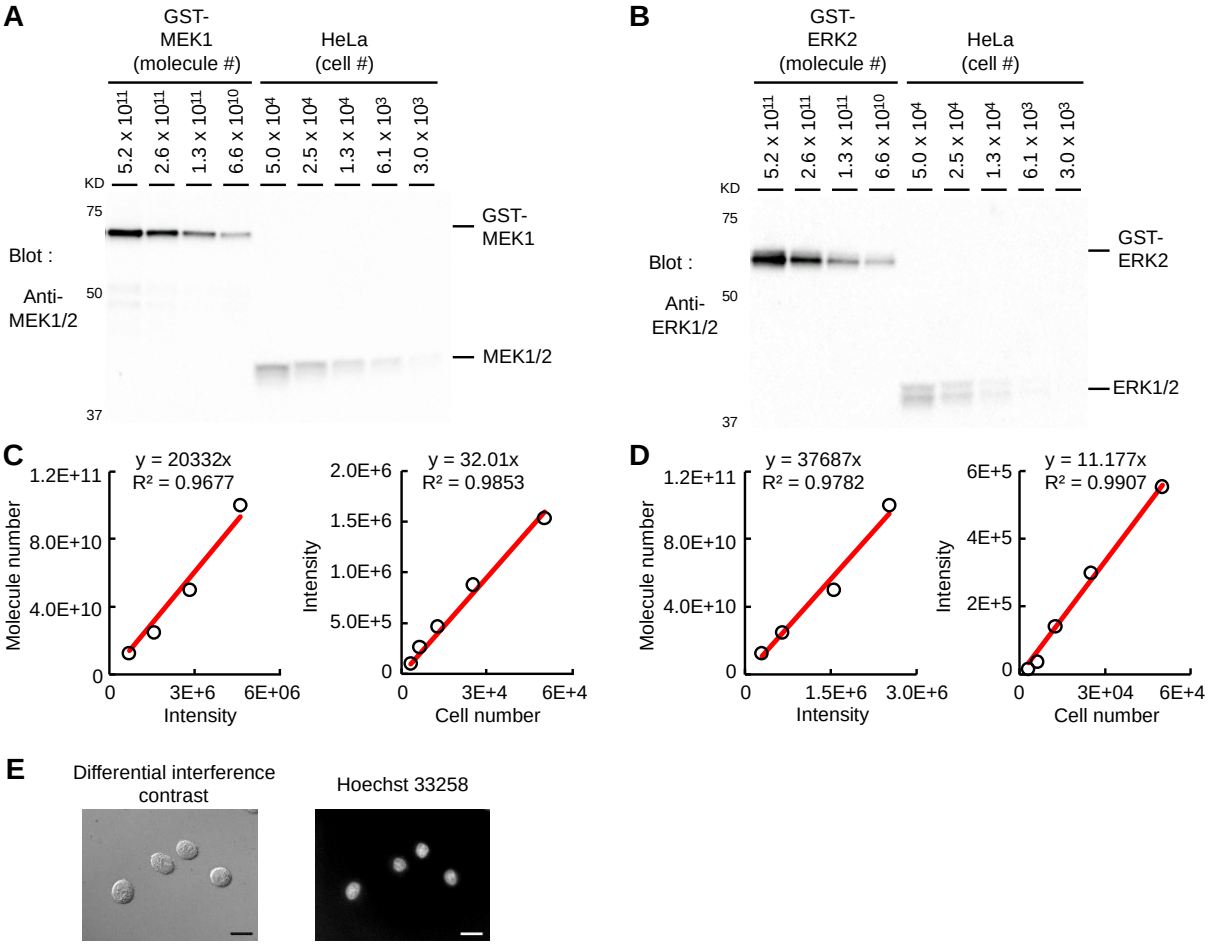

Fig. S1. Quantification of protein concentrations, dissociation constant, and nucleocytoplasmic shuttling rates. (A and B) For the determination of the molecule numbers of MEK and ERK, serial dilution of recombinant GST-tagged proteins and total cell lysates of HeLa cells were separated by SDS-PAGE, followed by immunoblotting with anti-MEK1/2 (A) and anti-ERK1/2 (B) antibodies. The bound antibodies were detected and quantified. (C and D) The bands in A and B were quantified and plotted as scatter plots, showing the linear relation between intensity and dilution of molecules and cell number. (E) For quantification of the volume of the cytoplasm and nucleus, HeLa cells were trypsinized and stained with Höechst 33258. Cells were imaged with differential interference contrast microscopy (upper, cytoplasm and nucleus) or fluorescence microscopy (lower, nucleus).

Fig. S2

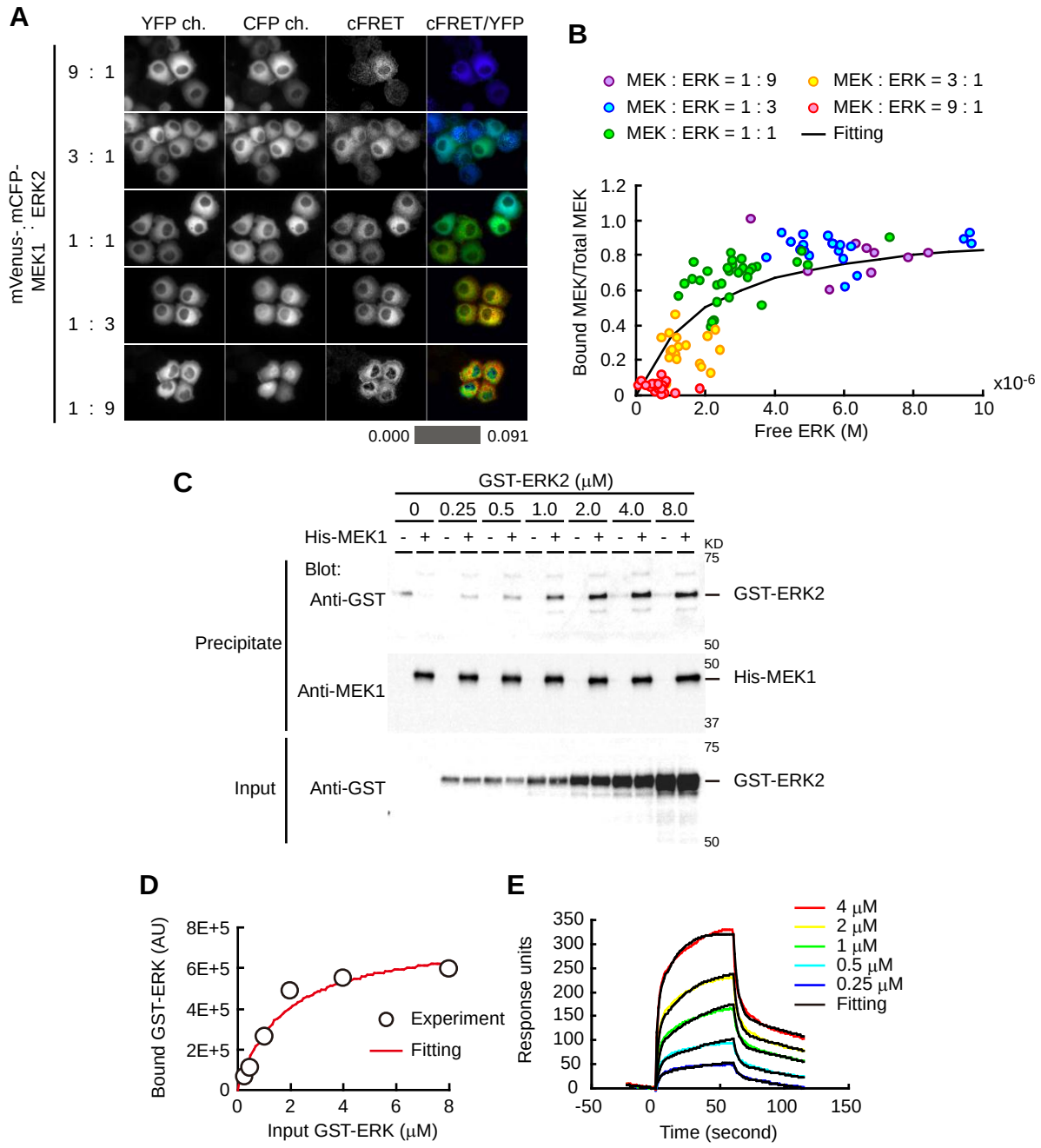

Fig. S2. Measurements of dissociation constant for the binding of MEK and ERK. (A) HeLa cells were transfected with plasmids encoding mVenus-MEK1 and mCFP-ERK2 as indicated ratio. Images of YFP, CFP and FRET were acquired two days after transfection. Then, corrected FRET image (cFRET) images were created by several corrections described in SI Materials and Methods. cFRET/YFP ratio images are shown in the intensity-modulated display mode, in which eight colors from red to blue are used to represent the cFRET/YFP ratio with the intensity of each color indicating the mean intensity of cFRET and YFP. The upper and lower limits of the ratio range are shown in the bottom. (B) Fraction of ERK-bound MEK (Bound MEK/Total MEK) versus the concentration of free ERK in each cell is plotted with the fitted curve. The dissociation constant was calculated as described in SI Materials and Methods. (C) Dissociation constant between MEK and ERK was measured by using in vitro binding assay. (D) The amount of bound versus free ERK is plotted with the fitted curve (Kd is 1.5 x 10^{-6} M). (E) Interaction between MEK and ERK was monitored in real time by surface plasmon resonance spectroscopy analysis. Increasing concentrations of ERK (0.25-4.0 x 10^{-6} M) were passed over a sensor chip with immobilized MEK for 60 s (association phase) before the flow was switched to buffer alone for another 60 s (dissociation phase). Association and dissociation rate constants were derived using BIAevaluation 4.1 software.

Fig. S3

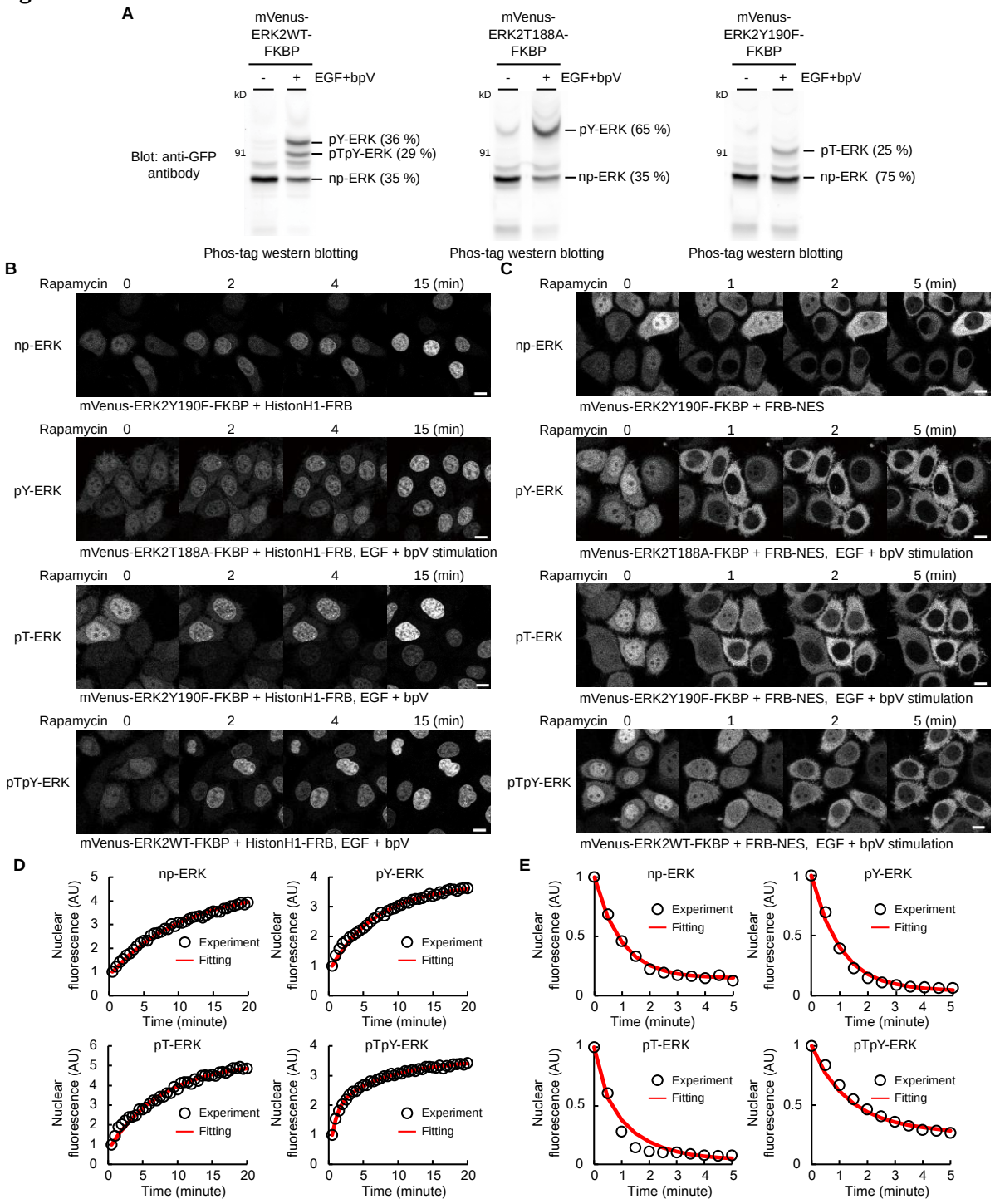

Fig. S3. Measurements of nucleocytoplasmic shuttling rates of phospho-isoforms of ERK. (A) HeLa cells expressing mVenus/FKBP-tagged ERK wild type (WT), T188A, or Y190F were serum-starved for 6-12 h and stimulated with 2.0 x 10^{-6} g/l EGF and 1.0 x 10^{-4} M bpV for 10 min. Cells were lysed and subjected to Phos-tag western blotting with anti-GFP antibody. The four phospho-isoforms of ERK are indicated on the right: np, non-phosphorylated; pT, threonine mono-phosphorylated; pY, tyrosine mono-phosphorylated; pTpY, threonine and tyrosine bis-phosphorylated (see Fig. S4 in detail). (B and C) HeLa cells expressing the proteins indicated at the bottom were stimulated with 2.0 x 10^{-6} g/l EGF and 1.0 x 10^{-4} M bpV for 10 min, followed by the addition of 2.5 x 10^{-7} M Rapamycin to trap the proteins at nucleus (B) or cytoplasm (C). (D and E) After Rapamycin treatment, the nuclear fluorescence intensity was monitored and fitted with single (np-ERK), double (pY-ERK, pT-ERK), or triple (pTpY-ERK) exponential curves. The fraction of each exponential curve was determined from the data shown in A. The nuclear import (D) and export (E) rates of each phospho-isoform was obtained from the time constants of the exponential curves.

Fig. S4

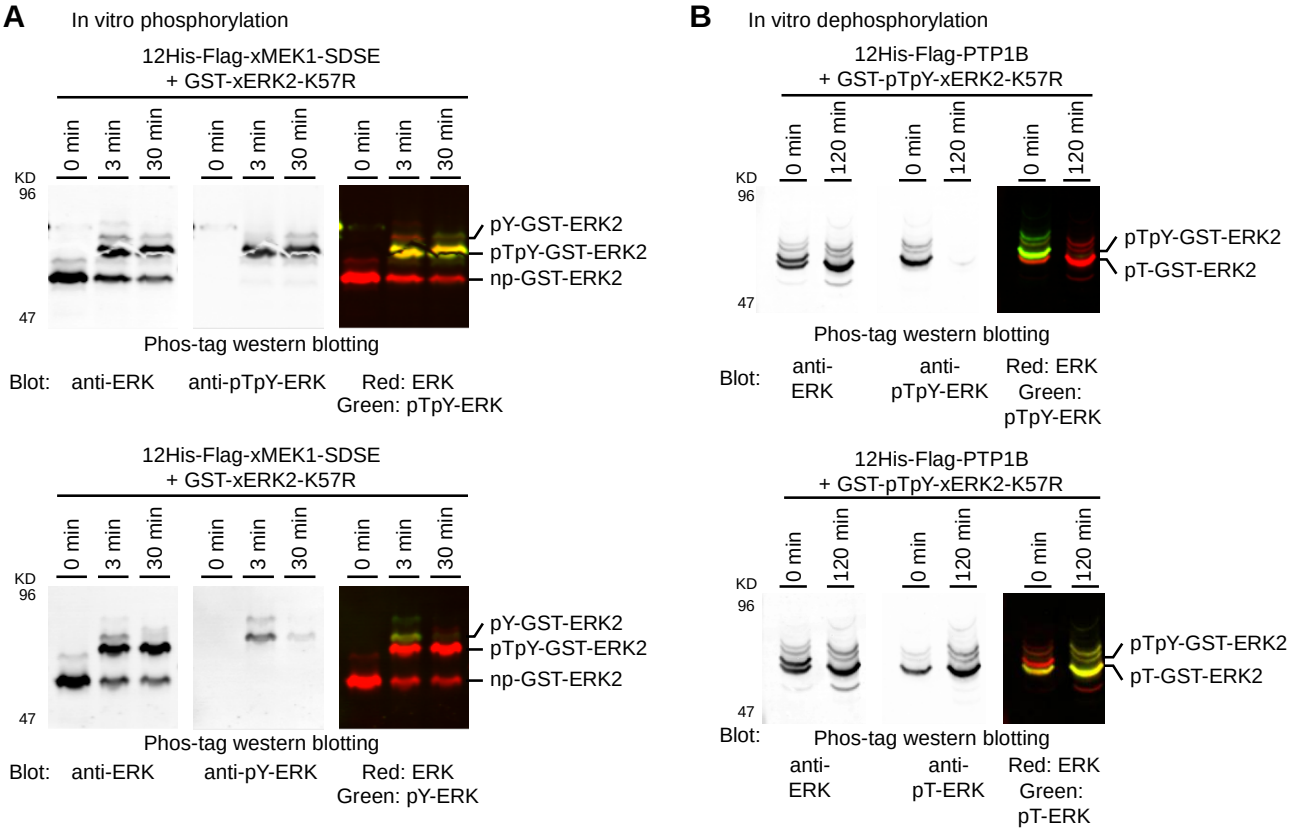

Fig. S4. Separation of phospho-isoforms of ERK by phospho-affinity gel electrophoresis. (A) GST-tagged Xenopus ERK2-KR (K57R, kinase-dead mutant) was phosphorylated in vitro by His-tagged Xenopus MEK1-SDSE (constitutively active mutant) for the indicated periods. Phosphorylated proteins were identified by Phos-tag western blot analysis with anti-ERK1/2 (upper and lower), anti-pTpY-ERK1/2 (upper), and anti-pY-ERK1/2 antibodies (lower). Non-phosphorylated ERK (np-ERK), tyrosine mono-phosphorylated ERK (pY-ERK), and tyrosine and threonine bis-phosphorylated ERK (pTpY-ERK) are denoted on the right. (B) GST-pTpY-ERK2 was dephosphorylated by His-tagged PTP1B to generate pT-ERK2. Phosphorylated proteins were analyzed by using anti-ERK1/2 (upper and lower), anti-pTpY-ERK1/2 (upper), and anti-pT-ERK1/2 antibodies (lower).

Fig. S5

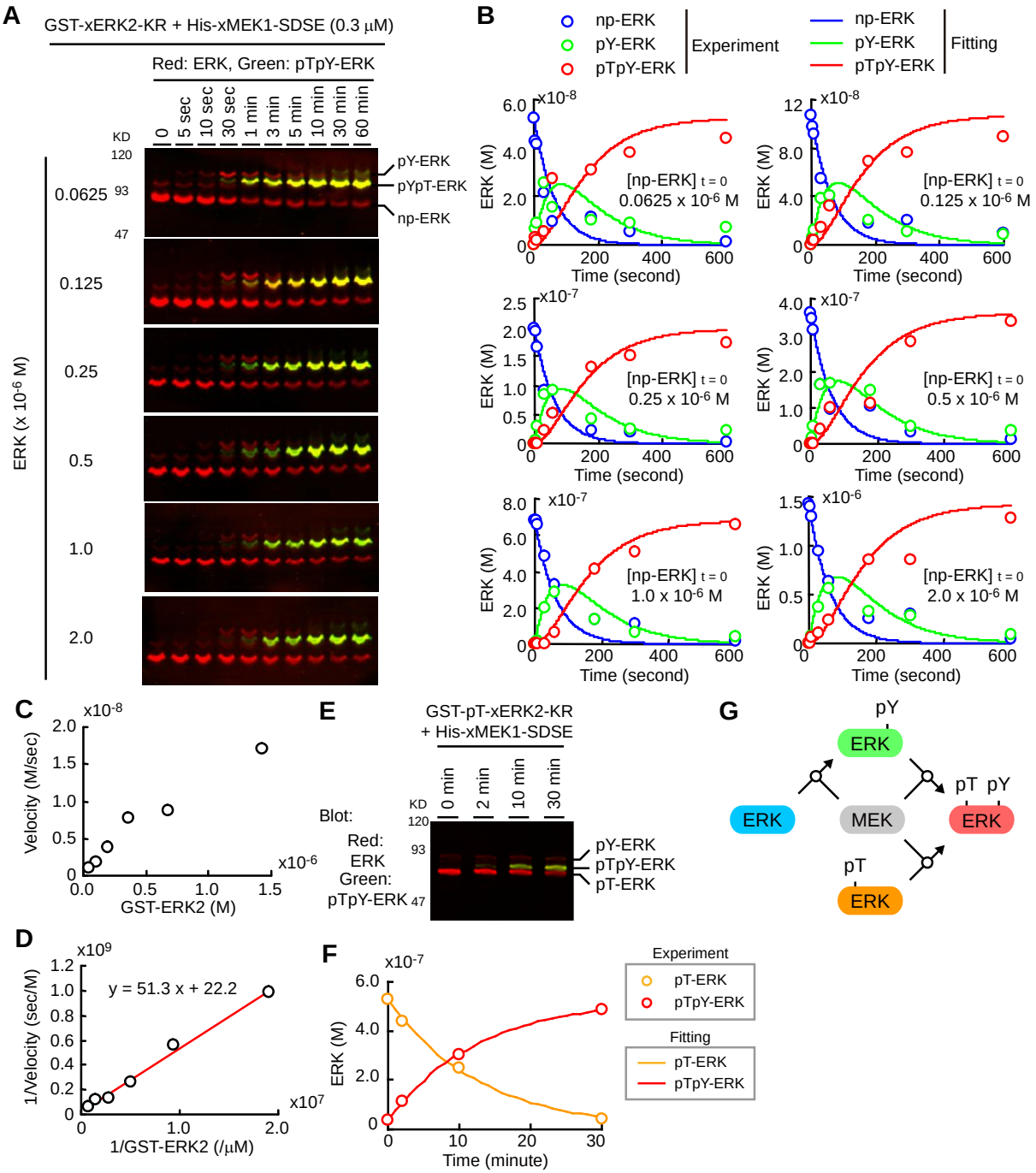

Fig. S5. Measurement of phosphorylation rates *in vitro*. (A) GST-ERK2-KR at the indicated concentrations was phosphorylated by His-tagged MEK1-SDSE (3.0×10^{-7} M) in the presence of 1.0×10^{-3} M ATP for the indicated time period, followed by Phos-tag western blot analysis. Non-phosphorylated ERK (np-ERK), tyrosine mono-phosphorylated ERK (pY-ERK), and tyrosine and threonine bis-phosphorylated ERK (pTpY-ERK) are denoted on the right. (B) The amounts of phospho-isoforms of ERK were quantified by subtracting the amount of non-reactive ERK, and plotted as circles. The data were fitted by a global least-square regression algorithm to a two-steps first-order phosphorylation model to obtain kinetic parameters. (C) The initial velocity of the first phosphorylation step is plotted against the substrate concentration. The velocity is not saturated in up to 1.5×10^{-6} M of substrate, indicating that the Michaelis constant of this phosphorylation step is larger than this range. (D) A Lineweaver-Burk plot of the first phosphorylation step is shown with the linear regression line. (E) GST-pT-ERK2-KR was phosphorylated by His-tagged MEK1-SDSE in the presence of 1.0×10^{-3} M ATP for the indicated period, followed by Phos-tag western blot analysis. (F) The amounts of phospho-isoforms of ERK were quantified and plotted. The data were fitted to a one-step first-order phosphorylation model to obtain kinetic parameters. (G) Schematic diagram of distributive ERK phosphorylation.

Fig. S6

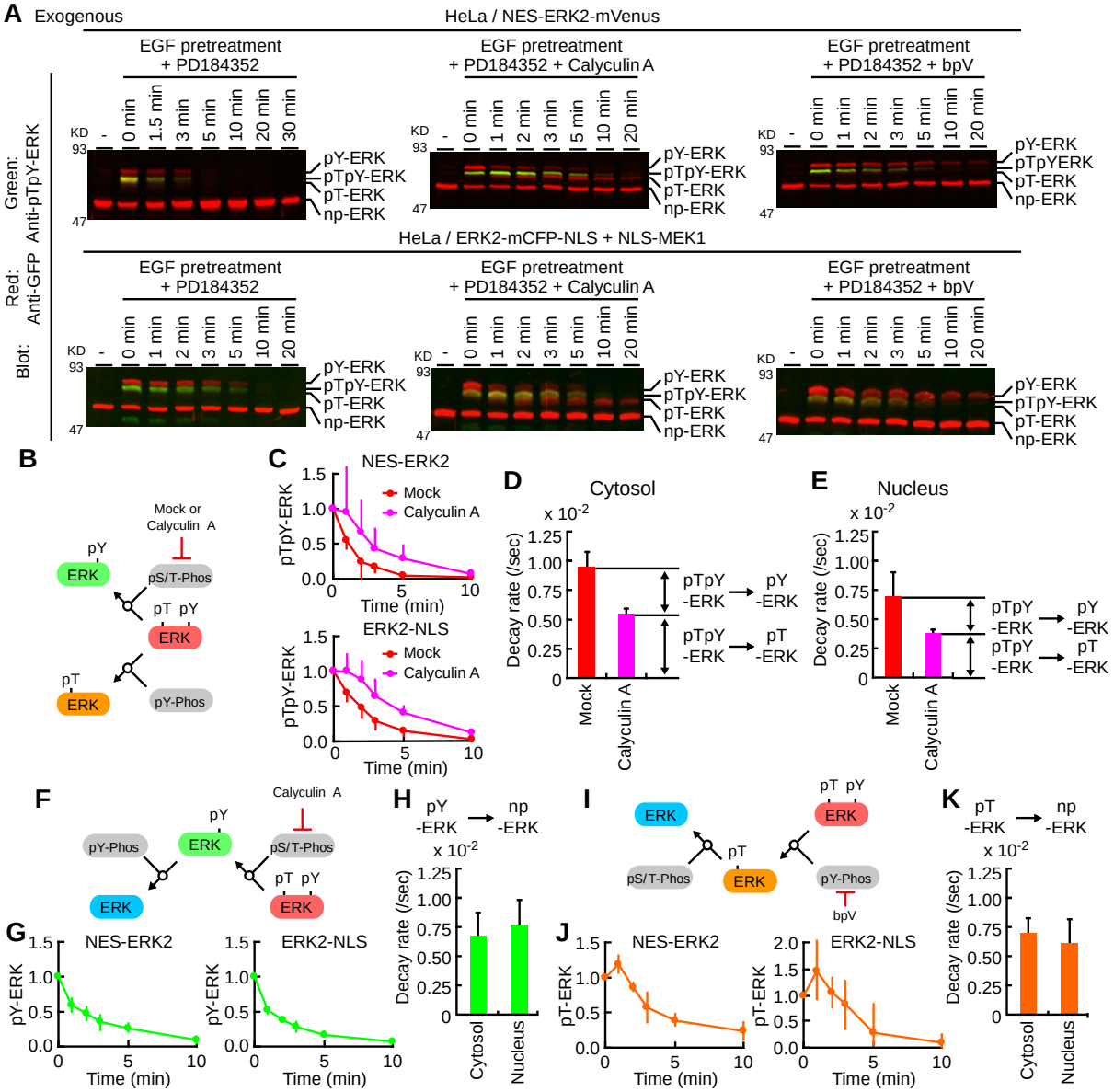

Fig. S6. Measurement of the dephosphorylation rate of ERK. (A) HeLa cells stably expressing NES-ERK2-mVenus (upper) or ERK2-mCFP-NLS with NLS-MEK1 (lower) were serum starved for 12 hours. Cells were left untreated or treated with 1.0 x 10^{-5} g/l EGF for 5 minutes, followed by 1.0 x 10^{-5} M PD184352 with mock (left), 1.0 x 10^{-7} M Calyculin A (center) or 1.0 x 10^{-4} M bpV (right) for the indicated time periods. Cell lysates were subjected to Phos-tag western blot analysis using anti-GFP and anti-pTpY-ERK antibodies. We repeated the same experiments four times with reproducible results, and representative results are shown. (B) Scheme of two dephosphorylation pathways for pTpY-ERK. (C) The decrease of pTpY-ERK after MEK inhibition by PD184352 in the presence or absence of Calyculin A was monitored in cytosol (upper) and nucleus (lower). Bars are SD (n = 4). (E and F) The dephosphorylation rates [/sec] in cytosol (D) and nucleus (E) were measured by fitting the time course of pTpY-ERK decay shown in C with an exponential decay function. Dephosphorylation rates from pTpY-ERK to pT-ERK were simply interpreted as the decay rates with Calyculin A. Dephosphorylation rates from pTpY-ERK to pY-ERK were obtained by subtracting total dephosphorylation rates from those of pTpY-ERK to pT-ERK. (F) Scheme of dephosphorylation pathways for pY-ERK. Calyculin A prevents an influx of pY-ERK via pTpY-ERK. (G) The decrease of pY-ERK upon MEK inhibition by PD184352 in the presence of Calyculin A was monitored in cytosol (left) and nucleus (right). Bars are SD (n = 4). (H) The dephosphorylation rates [/sec] in cytosol and nucleus were measured by fitting the time course of pY-ERK decay with an exponential function. (I) Scheme of dephosphorylation pathways for pT-ERK. bpV prevents an influx of pT-ERK via pTpY-ERK. (J) The decrease of pT-ERK upon MEK inhibition by PD184352 in the presence of bpV was monitored in cytosol (left) and nucleus (right). Bars are SD (n = 4). (K) The dephosphorylation rates [/sec] in cytosol and nucleus were measured by fitting the time course of pT-ERK decay with an exponential function. See SI Text in more details.

Fig. S7

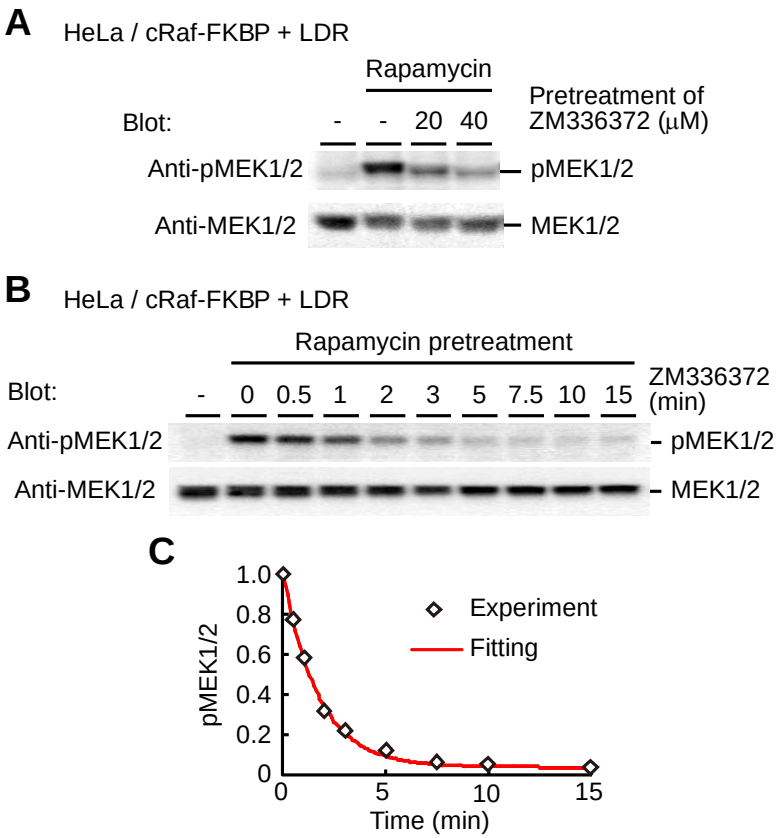

Fig. S7. Measurement of the dephosphorylation rate of MEK. To measure the MEK dephosphorylation rate in HeLa cells, we generated a HeLa cell line stably expressing cRaf-FKBP and LDR. Upon Rapamycin treatment of this cell line, cRaf-FKBP is recruited to plasma membrane and activated rapidly. Consequently, MEK is phosphorylated by the cRaf-FKBP without any perturbations of other signaling pathways. (A) The HeLa cells were left untreated or pretreated with a cRaf inhibitor, ZM336372, for 10 min, and then stimulated with Rapamycin for 30 min. The cell lysates were subjected to SDS PAGE and analyzed by anti-phospho-MEK1/2 (upper) and anti-MEK1/2 (lower) antibodies. (B and C) Measurement of the dephosphorylation rate of MEK. (B) The aforementioned HeLa cells were treated with or without Rapamycin for 15 min, and then treated with ZM336372 for the indicated time period. The cell lysates were collected and subjected to SDS-PAGE followed by immunoblotting analysis with anti-phospho-MEK1/2 (upper) and anti-MEK1/2 (lower) antibodies. These experiments were repeated three times and representative results are shown. (C) The relative amount of phosphorylated MEK1/2 was measured and plotted as a function of time after ZM336372 addition (min). The decay of MEK is fitted to the red line with a single exponential decay function.

Fig. S8

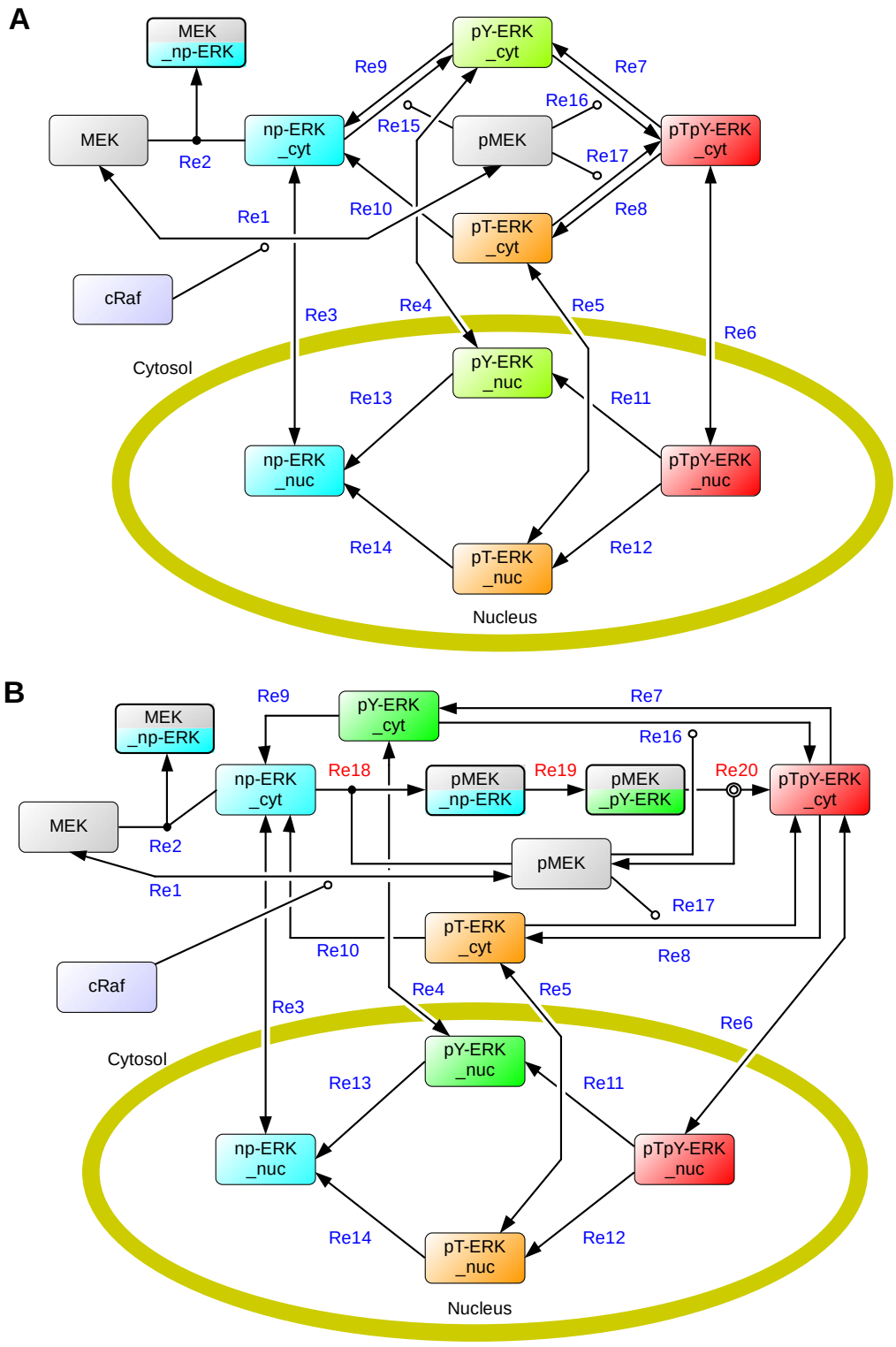

Fig. S8. Diagram of the distributive and processive model. (A) A process diagram of the distributive phosphorylation model of the MEK-ERK module was represented. The arrows represent the reactions (Re), which are numbered from 1 to 17 as described in the Table S2. (B) A process diagram of the processive phosphorylation model of the MEK-ERK module. The arrows represent the reactions (Re), which are numbered from 1 to 20 as described in the Table S2. Blue numbers are common between the distributive model and the processive model. Red numbers are reactions specific to the processive model.

Fig. S9

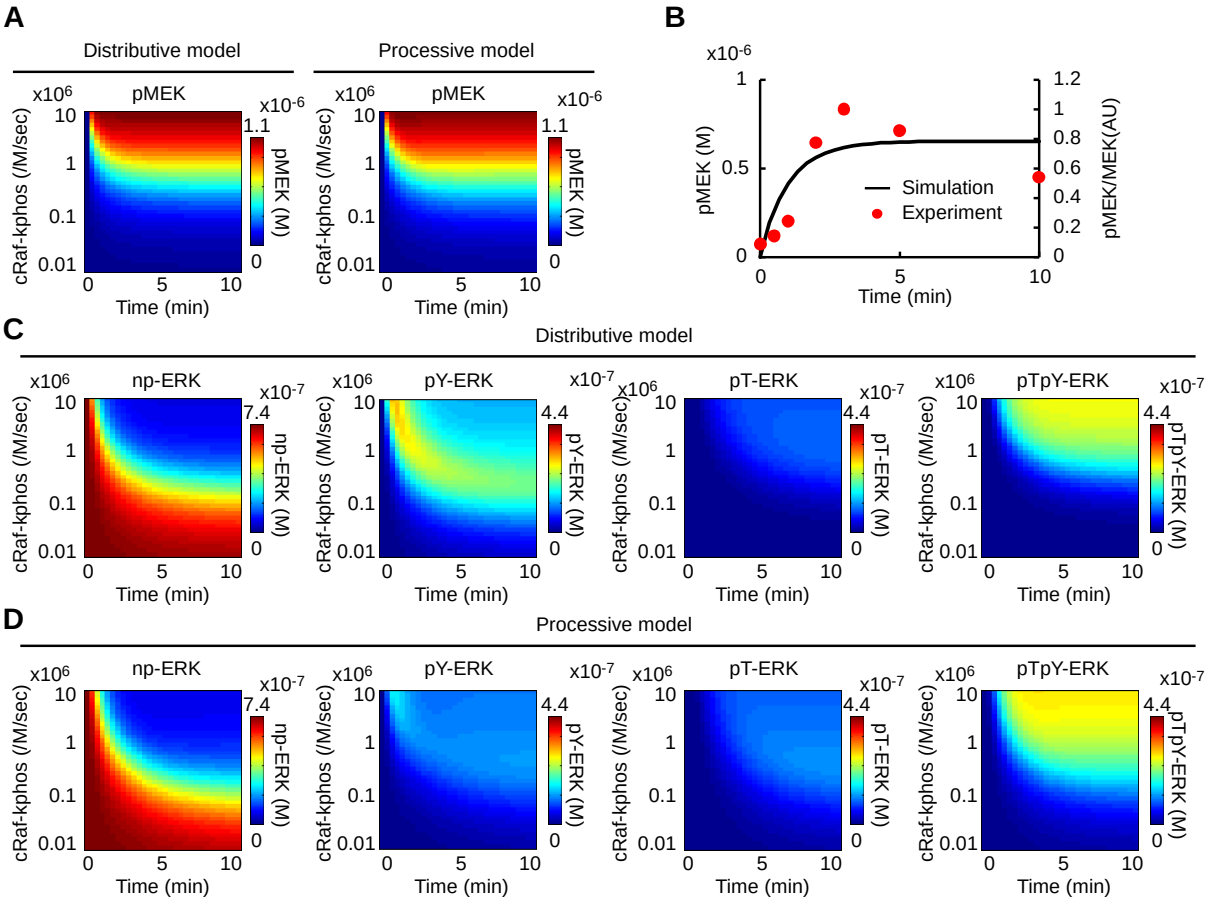

Fig. S9. Dynamics of ERK phosphorylation with varying MEK activity. Experimentally-determined parameters were used for the numerical simulations based on the distributive model and processive model. (A) Heat maps of the concentration of phosphorylated MEK upon stimulation in distributive model (left) and processive model (right). Horizontal and vertical axes indicate time after stimulation (minute) and kcat/Km value (Raf_kphos) of cRaf kinase for MEK phosphorylation as an input strength, respectively. (B) HeLa cells were stimulated with 1.0 x 10^{-5} g/l EGF, and lysed with SDS sample buffer at the indicated time points. The cell lysates were subjected to Western blotting analysis with anti-MEK1/2 and anti-phospho-MEK1/2 antibodies. The ratio of phospho-MEK to MEK (pMEK/MEK) is plotted against the time after EGF stimulation (red circle). In addition, the time course of MEK phosphorylation in the distributive model at kcat/Km value of 1.0 x 10^{6} [/M/sec] is superimposed in the same figure. (C and D) Shown here are the heat maps of the concentration of the indicated phospho-isoforms of ERK upon stimulation in the distributive model (C) and processive model (D).

Fig. S10

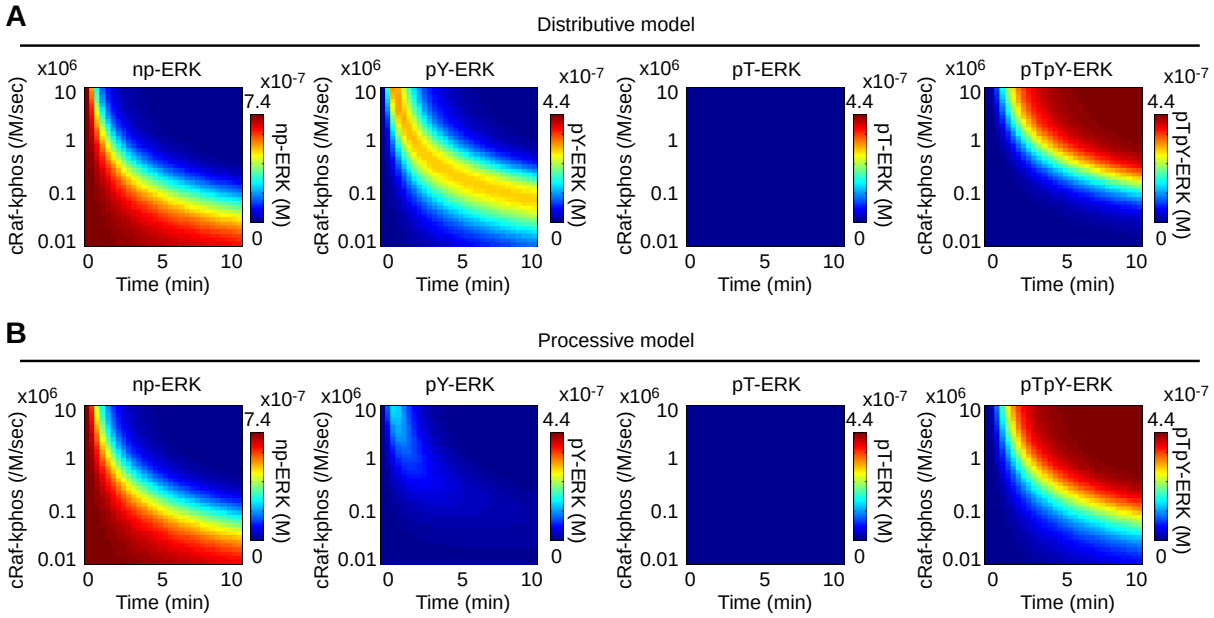

Fig. S10. Dynamics of ERK phosphorylation in the absence of dephosphorylation pathways. Shown here are heat maps of concentration of the indicated phospho-isoforms of ERK upon stimulation in the distributive model (A) and processive model (D) as well as shown in Figure S9 except for the lack of dephosphorylation pathways.

Fig. S11

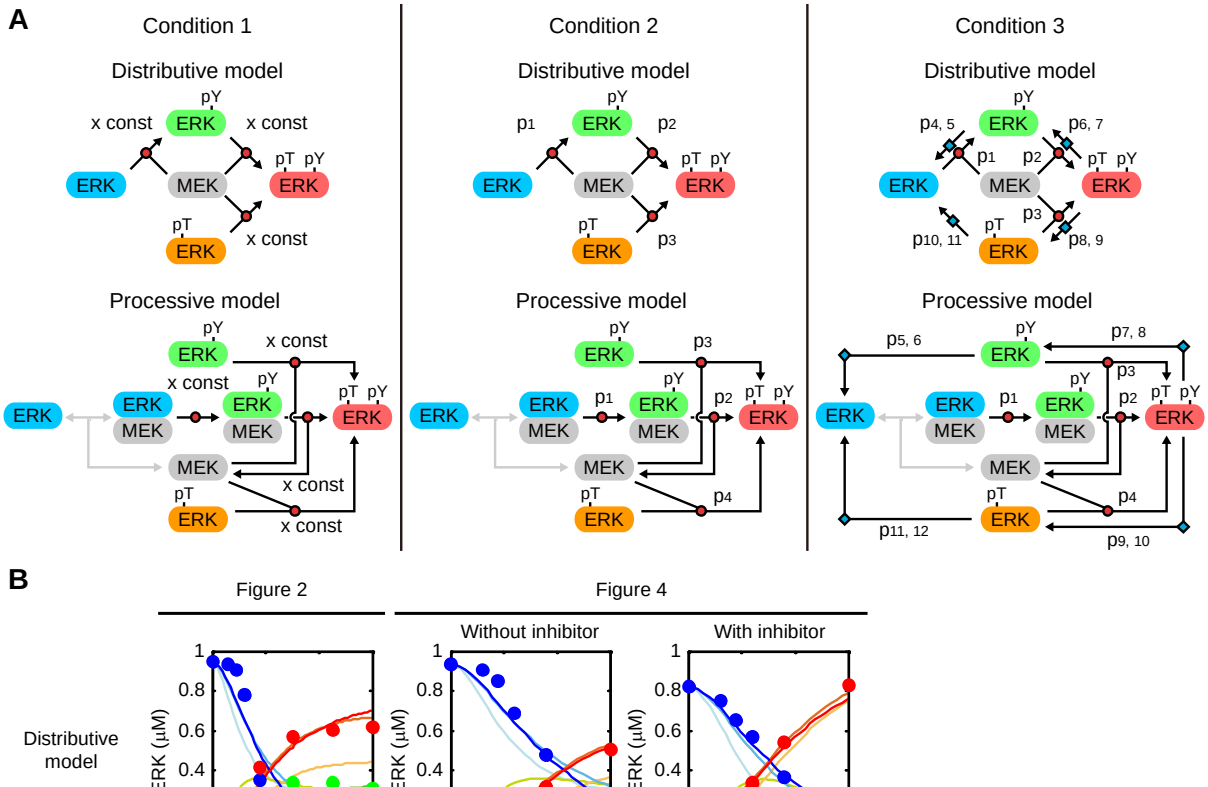

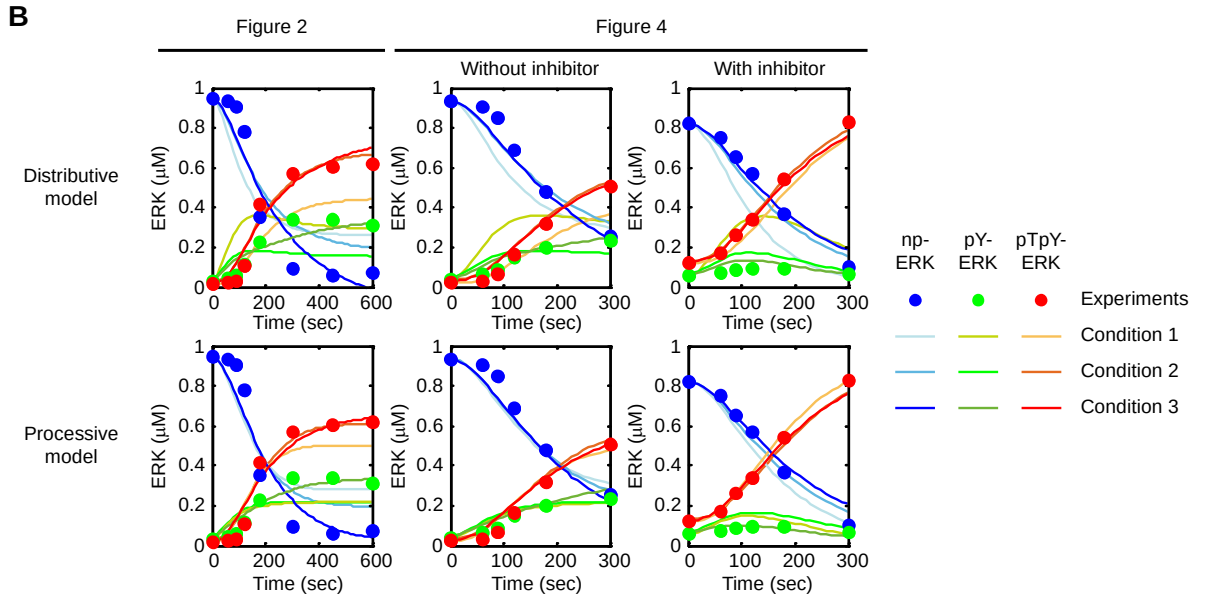

C

	Distributive model				Processive model			
	RSS	AIC	nH	Variables	RSS	AIC	nH	Variables
Condition 1	1.165	-36.3	1.66	1	0.421	-51.6	1.12	1
Condition 2	0.382	-49.0	1.79	3	0.275	-52.0	1.13	4
Condition 3	0.204	-42.5	2.27	11	0.180	-42.3	1.42	12

Fig. S11. Numerical validation of the processive phosphorylation model. (A) Numerical validation of the phosphorylation models by parameter fittings. (A) The conditions for the parameter fittings are illustrated. Black lines represent reactions to be optimized by parameter search. Condition 1 (left) aims to fit the data (Fig. 2E and Fig. 4D) by optimizing the quantity of the activated MEK; therefore the models have only 1 degree of freedom. Condition 2 (middle) aims to fit the data by independently changing the MEK activities against np-ERK, pY-ERK, and pT-ERK, allowing 3 and 4 degrees of freedom in the distributive and processive models, respectively. Condition 3 (right) aims to fit the data by changing all phosphorylation and dephosphorylation rates, allowing 11 and 12 degrees of freedom in the distributive and processive models, respectively. (B) The results of curve fitting are shown with the experimental data in Fig. 2E and Fig. 4D. (C) A table presents a summary of the parameter fitting. RSS, AIC, and nH refer to residual sum of square, Akaike information criterion, and Hill coefficient, respectively. Based on the AIC and Hill coefficient values, the processive model in Condition 2 is the most plausible model. In Condition 3, even though the AIC value of the distributive model is comparable to that of the processive model, the AIC value is much larger than that obtained for the processive model in Condition 2, suggesting over-fitting.

Fig. S12

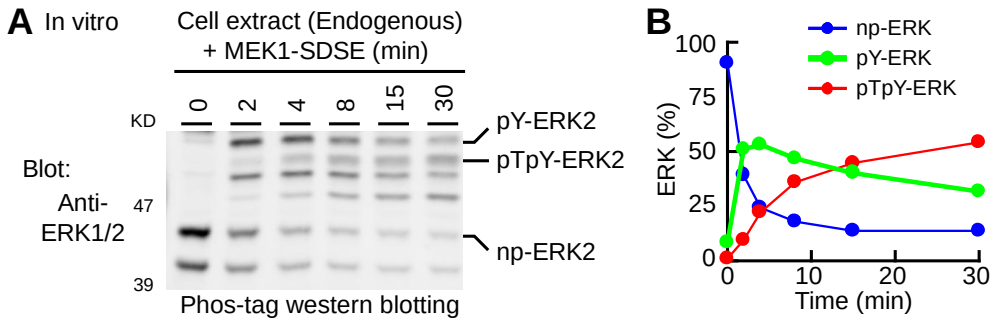

Fig. S12. In vitro ERK phosphorylation by using cell extract. Cytoplasmic extract prepared from HEK-293F cells were diluted with in vitro kinase buffer containing ATP and constitutively active MEK, and incubated for the indicated period (min). (A) The reaction solution were subjected to Phos-tag western blotting analysis. (B) The fractions of np-ERK2 (blue), pY-ERK2 (green), and pTpY-ERK2 (red) are plotted against time.

Fig. S13

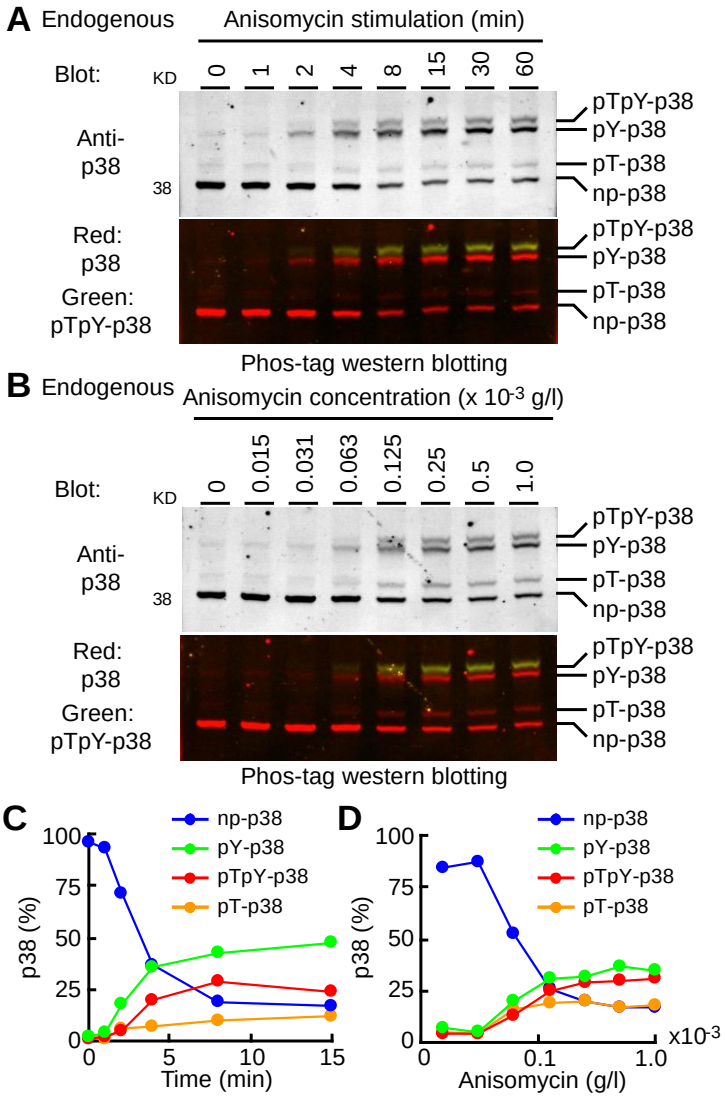

Fig. S13. Processive phosphorylation of p38 MAP kinase. (A) HeLa cells were stimulated with 1.0 x 10^{-3} g/l anisomycin at the indicated time. Cell lysates were subjected to Phos-tag western blot analysis. (B) HeLa cells were stimulated with indicated concentration of anisomycin for 30 min. Cell lysates were subjected to Phos-tag western blot analysis. (C and D) The phospho-isoforms of p38 in A and B were quantified and plotted. Notably, preceding accumulation of pY-p38, which was typical hallmark of distributive phosphorylation, was not observed in time-course (C) and steady-state (D) analysis.

Fig. S14

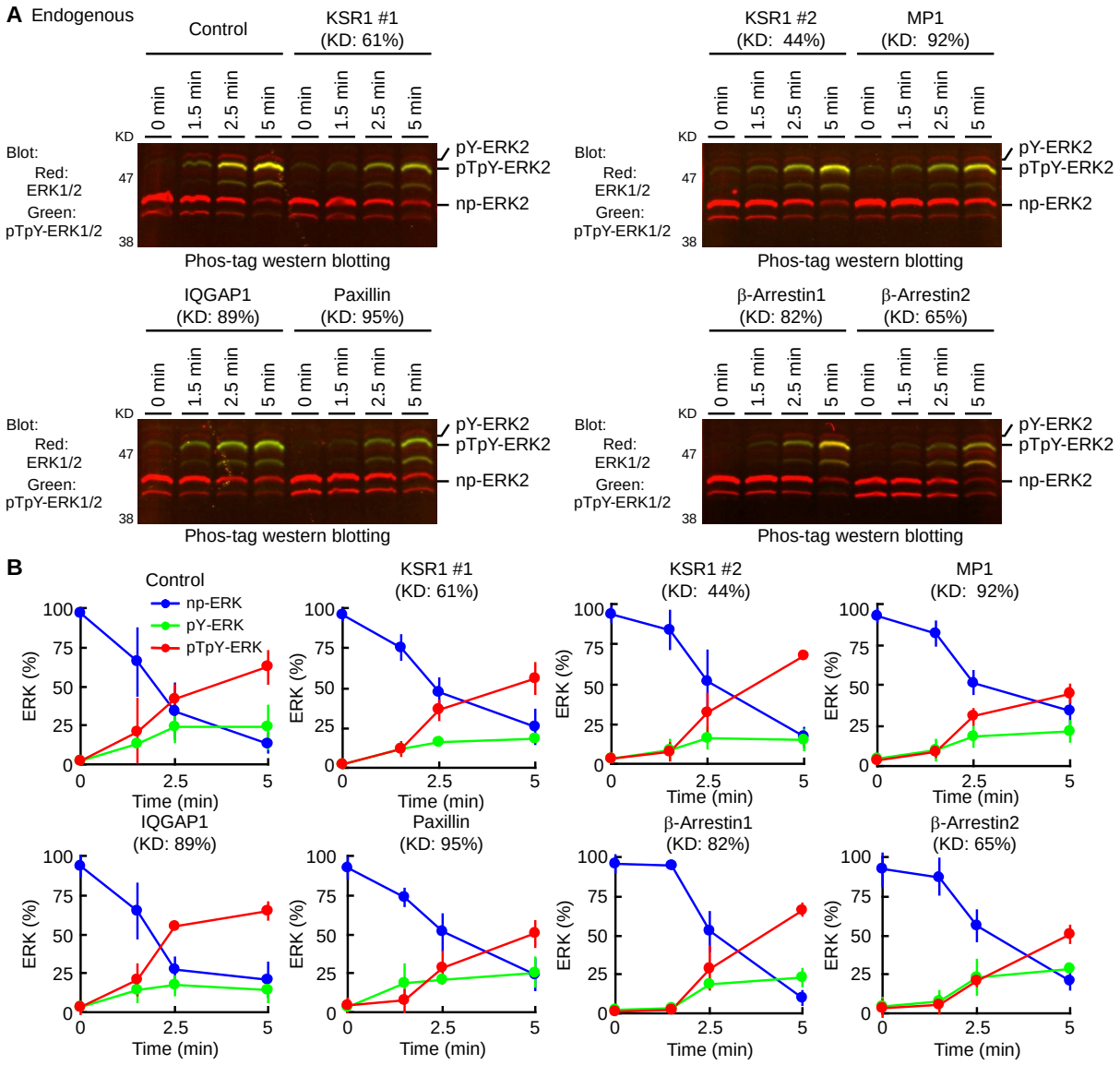

Fig. S14. Effects of scaffold proteins on the mode of ERK phosphorylation. (A) HeLa cells were transfected with siRNA for control or scaffold proteins as indicated. Three days after transfection, the HeLa cells were stimulated with 1.0 x 10^{-5} g/l EGF and analyzed at the indicated time. Cells were subjected to Phos-tag western blot analysis. Knockdown efficiency (KD, %) of siRNA was determined by quantitative RT-PCR analysis. (B) The phospho-isoforms of ERK quantified in A are plotted with SD (n = 3). See SI Text in more details.

Table S1

Table S1. Concentration of cRaf, MEK, and ERK in a HeLa cell.

Species	Concentration (M)			Comment
	Average	SD	N	
cRaf	1.3×10^{-8}	-	-	Fujioka et al. JBC 2006
MEK	1.2×10^{-6}	5.2×10^{-7}	3	Fig. S1
ERK	7.4×10^{-7}	3.3×10^{-7}	3	Fig. S1

Parameter	Volume (l)			Comment
	Average	SD	N	
Cytoplasm	2.8×10^{-12}	7.6×10^{-13}	20	Fig. S1
Nucleus	6.0×10^{-13}	2.1×10^{-13}	20	Fig. S1

MEK and ERK mean the total concentration of both MEK1 and MEK2 and both ERK1 and ERK2, respectively.

Table S2

Table S2. Kinetic models and parameters.

Reaction #	Reaction	Parameters					Comments
			Average	SD	Unit	N	
Re1	MEK + **cRaf** <=> pMEK	kf	1.0×10^{6}	-	/M/sec	-	Arbitrary
		kb	9.6×10^{-3}	2.2×10^{-3}	/sec	3	Fig. S7
Re2	MEK + np-ERK_cyt <=> MEK_np-ERK	kf	1.8×10^{5}	-	/M/sec	1	Fig. S2E[1]
		kb	2.7×10^{-1}	-	/sec	1	
Re3	np-ERK_cyt <=> np-ERK_nuc	kf	1.7×10^{-3}	5.5×10^{-4}	/sec	17	Fig. S3
		kb	1.3×10^{-2}	3.5×10^{-3}	/sec	7	Fig. S3
Re4	pY-ERK_cyt <=> pY-ERK_nuc	kf	2.5×10^{-3}	7.9×10^{-4}	/sec	19	Fig. S3
		kb	1.7×10^{-2}	4.6×10^{-3}	/sec	10	Fig. S3
Re5	pT-ERK_cyt <=> pT-ERK_nuc	kf	2.2×10^{-3}	9.9×10^{-4}	/sec	16	Fig. S3
		kb	4.9×10^{-2}	2.0×10^{-2}	/sec	7	Fig. S3
Re6	pTpY-ERK_cyt <=> pTpY-ERK_nuc	kf	8.2×10^{-3}	5.7×10^{-3}	/sec	15	Fig. S3
		kb	7.6×10^{-3}	3.6×10^{-3}	/sec	16	Fig. S3
Re7	pTpY-ERK_cyt -> pY-ERK_cyt	kf	4.0×10^{-3}	8.5×10^{-4}	/sec	4	Fig. S6
Re8	pTpY-ERK_cyt -> pT-ERK_cyt	kf	5.5×10^{-3}	4.7×10^{-4}	/sec	4	Fig. S6
Re9	pY-ERK_cyt -> np-ERK_cyt	kf	6.7×10^{-3}	2.0×10^{-3}	/sec	4	Fig. S6
Re10	pT-ERK_cyt -> np-ERK_cyt	kf	6.8×10^{-3}	1.1×10^{-3}	/sec	4	Fig. S6
Re11	pTpY-ERK_nuc -> pY-ERK_nuc	kf	3.2×10^{-3}	1.7×10^{-3}	/sec	4	Fig. S6
Re12	pTpY-ERK_nuc -> pT-ERK_nuc	kf	3.8×10^{-3}	3.0×10^{-4}	/sec	4	Fig. S6
Re13	pY-ERK_nuc -> np-ERK_nuc	kf	7.7×10^{-3}	2.1×10^{-3}	/sec	4	Fig. S6
Re14	pT-ERK_nuc -> np-ERK_nuc	kf	5.8×10^{-3}	2.2×10^{-3}	/sec	4	Fig. S6
Re15	np-ERK_cyt + **pMEK** -> pY-ERK_cyt	kf	3.9×10^{4}	1.9×10^{4}	/M/sec	2	Fig. S5[2]
Re16	pY-ERK_cyt + **pMEK** -> pTpY-ERK_cyt	kf	2.1×10^{4}	1.1×10^{4}	/M/sec	2	Fig. S5[2]
Re17	pT-ERK_cyt + **pMEK** -> pTpY-ERK_cyt	kf	2.0×10^{4}	-	/M/sec	1	Fig. S5
Re18	pMEK + np-ERK_cyt <=> pMEK_np-ERK	kf	1.8×10^{5}	-	/M/sec	-	Assumption[3]
		kb	2.7×10^{-1}	-	/sec	-	
Re19	pMEK_np-ERK -> pMEK_pY-ERK	kf	7.3×10^{-2}	- -	/sec	-	Calculated from Re15 and Re 18[4]
Re20	pMEK_pY-ERK -> pTpY-ERK_cyt + pMEK	kf	5.0×10^{-2}	-	/sec	-	Estimated from Figure 2E

The reaction number is indicated in Figure S8A and S8B. Bold character means enzyme. The symbols <=> and -> indicate a reversible reaction and an irreversible reaction, respectively. kf and kb are forward and reverse kinetic parameters, respectively.

[1] kf and kb are obtained by Biacore with 5 different sets of ligand concentration. Dissociation constants, which are measured by FRET and in vitro binding assay, are 1.7 x 10^-6 ± 6.8 x 10 ^-7 [M] (N = 3) (Fig. S2A and B) and 1.8 x 10^-6 [M] (N = 1) (Fig. S2C and D), respectively.

[2] Parameters are obtained by global fitting of 2 independent experiments with 10 different sets of substrate and enzyme concentration.

[3] Assuming that the association/dissociation rate constants of the binding bewtween pMEK and ERK are comparable with them of the binding of MEK and ERK.

[4] kcat/Km = kcat/(kb+kcat)/kf, and then 0.038 = kcat/(0.27+kcat)/1.8. Thus, kcat = 0.79.

Table S3

Table S3. Summary of parameters fitted with three different conditions in Figure S11.

Reaction #	Reaction	Initial value (Unit)		Fitting condition 1		Fitting condition 2		Fitting condition 3	
				Distributive	Processive	Distributive	Processive	Distributive	Processive
Re7	pTpY-ERK_cyt -> pY-ERK_cyt	kf	4.0×10^{-3} /sec					6.5×10^{-3}	9.2×10^{-3}
Re8	pTpY-ERK_cyt -> pT-ERK_cyt	kf	5.5×10^{-3} /sec					-6.1×10^{-3}	-3.0×10^{-4}
Re9	pY-ERK_cyt -> np-ERK_cyt	kf	6.7×10^{-3} /sec					6.8×10^{-3}	-1.2×10^{-3}
Re10	pT-ERK_cyt -> np-ERK_cyt	kf	6.8×10^{-3} /sec					7.7×10^{-3}	1.0×10^{-3}
Re11	pTpY-ERK_nuc -> pY-ERK_nuc	kf	3.2×10^{-3} /sec					1.0×10^{-3}	2.8×10^{-3}
Re12	pTpY-ERK_nuc -> pT-ERK_nuc	kf	3.8×10^{-3} /sec					8.6×10^{-3}	-2.3×10^{-3}
Re13	pY-ERK_nuc -> np-ERK_nuc	kf	7.7×10^{-3} /sec					-4.5×10^{-3}	7.8×10^{-3}
Re14	pT-ERK_nuc -> np-ERK_nuc	kf	5.8×10^{-3} /sec					1.7×10^{-3}	6.9×10^{-3}
Re15	np-ERK_cyt +**pMEK** -> pY-ERK_cyt	kf	3.9×10^{4} /M/sec	2.9×10^{4}		1.7×10^{4}		1.4×10^{4}	
Re16	pY-ERK_cyt +**pMEK** -> pTpY-ERK_cyt	kf	2.1×10^{4} /M/sec	1.6×10^{4}	1.3×10^{4}	3.9×10^{4}	1.6×10^{4}	4.6×10^{4}	2.0×10^{4}
Re17	pT-ERK_cyt +**pMEK** -> pTpY-ERK_cyt	kf	2.0×10^{4} /M/sec	1.4×10^{4}	1.2×10^{4}	2.8×10^{7}	3.6×10^{7}	2.3×10^{4}	3.3×10^{4}
Re19	pMEK_np-ERK -> pMEK_pY-ERK	kf	7.9×10^{-2} /sec		4.7×10^{-2}		3.9×10^{-2}		3.2×10^{-2}
Re20	pMEK_pY-ERK -> pTpY-ERK_cyt + pMEK	kf	5×10^{-2} /sec		3.0×10^{-2}		2.3×10^{-2}		4.2×10^{-2}

The reaction number is indicated in Figure S8A and S8B. Bold character means enzyme. The symbols <=> and -> indicate a reversible reaction and an irreversible reaction, respectively. kf and kb are forward and reverse kinetic parameters, respectively.